Investigation of spin-orbit torque efficiency in CuBi alloys

Katsuhiro Tatsuoka,[1] Motomi Aoki,[1] Mitsuru Funato,[1] Ryo Ohshima,[1,2] Yuichiro Ando,[1,2,3] and Masashi Shiraishi[1,2,*]

[1]*Department of Electronic Science and Engineering, Kyoto University, Nishikyo-ku, Kyoto 615-8510, Japan*

[2]*Center for Spintronics Research Network (CSRN), Kyoto University, Gokasho, Uji, Kyoto 611-0011, Japan*

[3]*PRESTO, Japan Science and Technology Agency, Honcho, Kawaguchi, Saitama 332-0012, Japan*

(Received 5 April 2024; revised 16 August 2024; accepted 19 August 2024; published 11 September 2024)

Experimental demonstration of substantially large and negative spin Hall angle in CuBi alloys, in which diluted Bi atoms are doped into Cu, sheds light on a novel aspect of spin-charge interconversion physics using Bi, where much effort has been paid to explore large spin-charge interconversion efficiency expected from the gigantic spin-orbit interaction of Bi. Since the spin Hall effect allows concomitant spin-orbit torque (SOT) that is a significant trait in spintronic phenomena for applications, an investigation of the spin-orbit torque efficiency in CuBi, that has not been thoroughly studied, is an important challenge. In this study, we estimate the SOT efficiency of CuBi by suppressing unwanted spin backflow. Surprisingly, the sign of the SOT efficiency is positive, unlike that in previous work. The amplitude of the SOT efficiency decreases monotonically as a function of the Bi composition of the CuBi alloy, which is attributed to the interplay of the orbital Hall effect of Cu and the interfacial Rashba effect in the SOT devices.

DOI: 10.1103/PhysRevB.110.094419

I. INTRODUCTION

The sizable spin-orbit interaction (SOI) of bismuth (Bi) gives rise to a wide variety of intriguing physics and has been attracting attention. One of the most notable physical traits of Bi induced by its SOI is spin-charge interconversion (SCI), in which spin current is converted to charge current and vice versa [1,2]. Since the advent of SCI physics, much effort has been devoted to realizing efficient charge-spin conversion using Bi because Bi has the largest SOI among nonradioactive elements. However, previous attempts to achieve SCI using Bi seem to refute the aforementioned statement, because the SCI efficiency of Bi differs between studies [3–6], and more surprisingly, is much lower than that of platinum (Pt) [7–12], tantalum [13,14], and tungsten [15], which have smaller SOI than Bi. An example that illustrates this intricate situation is the absence of a SCI effect in Bi(111) single crystals, whereas the spin Seebeck effect in the ferrimagnetic insulator yttrium-iron-garnet (YIG) generated a spin current that was injected into Bi [16]. Because the Bi(111) crystal on YIG was immune to spin injection and its possible inverse spin Hall effect, insurmountable obstacles for realization of efficient SCI might have existed in the material.

A recent study shedding light on the g-factor anisotropy of Bi provided a distinct picture to realize efficient SCI [17], where the large g-factor of carriers in Bi(110) can allow the exhibition of sizable SCI (0.17–0.27) by spin-torque ferromagnetic resonance (STFMR) measurements [9,18] and second harmonic Hall (SHH) measurements [19–21], whereas the SCI efficiency in Bi(111) was negligible. Similar large SCI efficiency was also realized in CuBi alloys, in which Bi atoms were doped into copper (Cu) [22–28]. Cu is well known as a weak SOI element with a low SCI efficiency unless it experiences oxidation [29]. The recent discovery of a discernible orbital Rashba-Edelstein effect provides a fuller understanding of the spintronic and magnetic physics of Cu oxide [30,31]. Furthermore, the orbital Hall effect (OHE) [32] can broaden the horizons of spintronic traits of bulk pure Cu. However, Bi doped into Cu can play a dominant role in SCI; the conversion efficiency of CuBi alloys is reported to be -0.08 to -0.24 because of skew scattering [23]. In addition, iridium [23,33,34] and Pt [35] can also play a similar role when doped in Cu, which indicates that heavy elements can behave as spin-scattering centers and allow efficient SCI in an atomic form. It is also notable that Bi-doped silicon can display weak antilocalization because of the SOI of Bi [36].

Once efficient SCI using Bi is established, the research target can be expanded towards introducing the efficient SCI of Bi into spintronic devices and obtaining deeper insight into related spin physics. To delve further into the subject of SCI in Bi, here we investigate the spin-orbit torque (SOT) efficiency of CuBi in SOT devices using the STFMR and SHH methods. To avoid underestimation of the SOT efficiency caused by spin backflow [9], a spin sink (SS) layer is included below the CuBi layer in the SOT devices. The Bi composition dependence of the CuBi can rationalize that the sign of the SOT from the CuBi/Pt devices is positive and its possible underlying physics is discussed.

II. SAMPLE FABRICATION AND EXPERIMENTAL SETUP

For the STFMR and SHH measurements, channel patterns for coplanar waveguides and Hall bar patterns were fabricated on an MgO(100) substrate (Tateho Chemical Industries Co.,

*Contact author: shiraishi.masashi.4w@kyoto-u.ac.jp

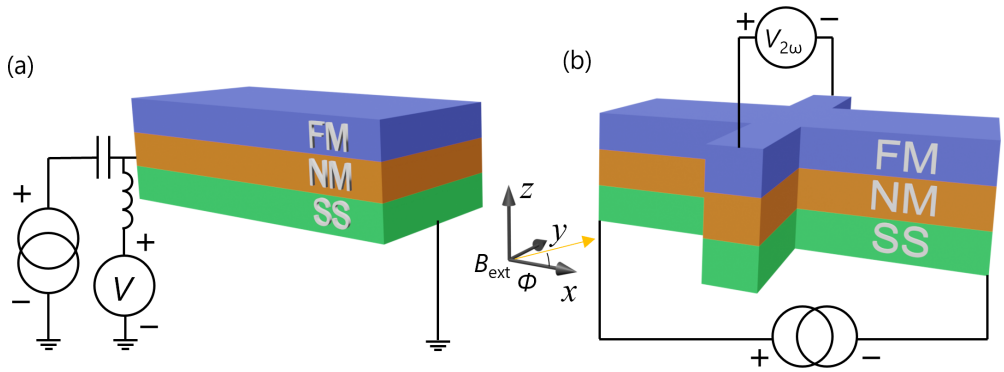

FIG. 1. Schematics of the devices and setups for (a) spin-torque ferromagnetic resonance (STFMR) and (b) second harmonic Hall (SHH) measurements. In the STFMR measurements, a dc voltage is measured through a bias tee under the application of an ac electric current while an external magnetic field B_{ext} is applied along the ϕ direction. In the SHH measurements, the SHH voltage is measured using a lock-in amplifier under the application of an ac electric current while an external magnetic field B_{ext} is applied along the ϕ direction.

Ltd.) coated with PMMA resist (KAYAKU Advanced Materials, Inc.) and 300Z ESpacer (Resonac Holdings Corp.) by electron-beam lithography. An SiO_2(7)/FM(5)/CuBi(5)/Pt(5) film (numbers in parentheses are the thickness in nanometers; FM is ferromagnet) was deposited *in situ* using rf sputtering on an MgO substrate. Co or permalloy (Py; $Ni_{80}Fe_{20}$) was used as an FM and the Bi composition ratio x of CuBi ($Cu_{100-x}Bi_x$) (Furuuchi Chemical Corp.) was set to $x = 0$, 0.3, 0.5, 1, 3, and 6. For structural characterization, transmission electron microscopy (TEM) observations of the SiO_2(7)/Co(5)/$Cu_{99.5}Bi_{0.5}$(5)/Pt(5) trilayer were carried out under an acceleration voltage of 200 kV using a JEM-2100F (JEOL). The TEM specimens were prepared by Ar ion milling. Compositions of the elements were measured by energy dispersive x-ray spectroscopy (EDX). Before depositing Au/Ti to fabricate coplanar waveguides and electrodes for Hall bar patterns by electron-beam deposition, contact areas were milled both *ex situ* and *in situ* to remove the SiO_2 capping layer. A Pt layer was inserted as an SS layer to suppress spin backflow from the CuBi layer (see the following section for details). The SOT efficiency of the devices was evaluated by STFMR and SHH measurements.

The device structure and setup for the STFMR measurements are shown in Fig. 1(a). Microwaves were applied using a signal generator (Keysight, N5173B). The input power was set to 10 mW for the devices with $x = 0$, 0.3, 0.5, and 1, and 20 mW for $x = 3$ and 6, which is because higher input power was required to observe clear spectra for devices with the higher x because of their higher resistivity. In all measurements, the direct current (dc) voltage was detected using a nanovoltmeter (Keithley, 2182A) through a bias tee (Keysight, 11612A).

The SHH measurements were carried out using a physical property measurement system (Quantum Design, PPMS). The SHH voltages were measured using the setup shown in Fig. 1(b). An alternating current (ac) with an amplitude of $I_0 = 20$ mA and frequency of 17 Hz was applied using a current source (Keithley, 6221). The SHH and first harmonic Hall voltages were measured simultaneously using a lock-in amplifier (Stanford Research Systems, SR830). All measurements were conducted at room temperature.

III. RESULTS AND DISCUSSION

Figure 2 shows the TEM image and the result of EDX of the SiO_2(7)/Co(5)/$Cu_{99.5}Bi_{0.5}$(5)/Pt(5) trilayer structure. The contrast of each layer in the TEM image is seen [see Figs. 2(a) and 2(b)] and, in addition, the EDX spectra of Co, CuBi, and Pt are discernible and correspond to the film thicknesses. It is notable that the atomic numbers of Co and Cu are almost the same, which hinders detecting a clear Co/CuBi interface in the TEM observation and that the peak broadening of the EDX signals is attributed to the fact that incident electrons into the layer can diffuse in the sample (see also Supplemental Material, Sec. D [37] and Refs. [38,39] therein for the details). Whereas the EDX result can underpin our assertion that there is no significant intermixing of the Co, CuBi, and Pt in the sample, formation of an intermixing layer such as Cu and Pt (Cu:Pt) is not completely negated from the TEM and EDX results shown in Fig. 2, which may give rise to a concomitant SCI effect. Regarding the EDX spectrum of Bi, it was not detectable likely due to its small composition in Cu. Albeit unequivocal evidence is not obtained, the results shown in Fig. 2 can signify that interdiffusion of the Bi to the other layers is not probable.

The spin diffusion length (λ) in CuBi is reported to be several tens of nanometers despite its giant spin Hall angle [23], which leads to considerable suppression of the SOT signals because of spin backflow [Fig. 3(a)]. To circumvent this problem, it is necessary to insert an SS layer to enable observation of the SOT of devices consisting of an FM/nonmagnet (NM) bilayer [see Fig. 3(b)], especially when the spin diffusion length of the NM layer is long. Indeed, a previous study showed that an SS layer enhances the SOT signal originating from the NM layer [40]. To clarify how the SS layer enables observation of the SOT originating from the CuBi layer, we calculated the SOT in Co(5)/$Cu_{99.5}Bi_{0.5}$(5) and Co(5)/$Cu_{99.5}Bi_{0.5}$(5)/Pt(5) structures using a spin diffusion model [41]. The resistivities (ρ) of Co and Pt used in our calculation were measured to be $\rho_{Co} = 99.0\ \mu\Omega$ cm and $\rho_{Pt} = 38.5\ \mu\Omega$ cm, respectively, by the four-probe method. The resistivity of CuBi (ρ_{CuBi}) of 20.8 $\mu\Omega$ cm was estimated from the resistance of Co(5)/$Cu_{99.5}Bi_{0.5}$(5)/Pt(5) using a parallel circuit model. The spin diffusion lengths of Co and Pt were set as

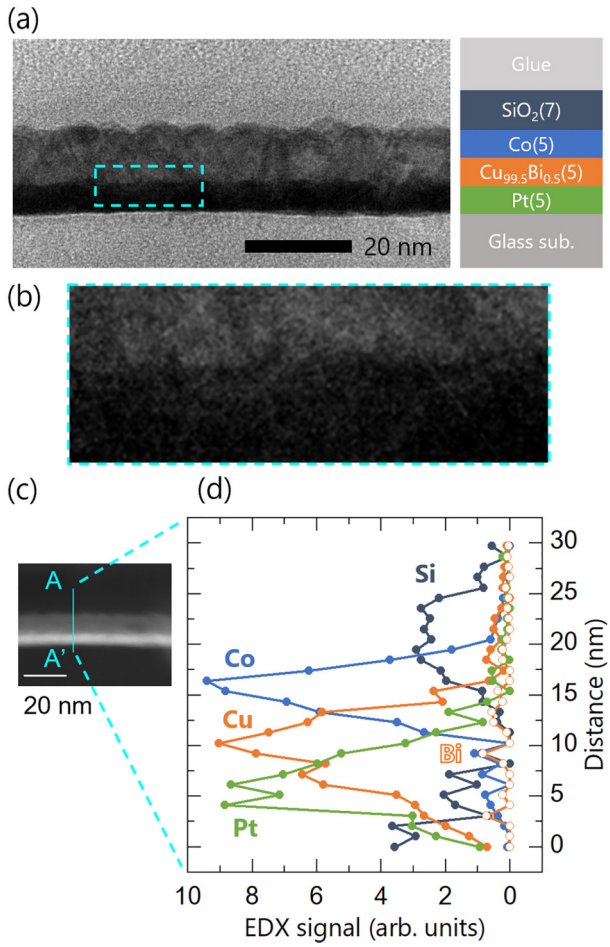

FIG. 2. (a) TEM image of SiO_2(7)/Co(5)/$Cu_{99.5}Bi_{0.5}$(5)/Pt(5) grown on a glass substrate and its corresponding schematic. (b) Enlarged view of the $Cu_{99.5}Bi_{0.5}$/Pt interface of the area enclosed by light blue dotted line shown in (a). (c) High-angle annular dark field scanning TEM (HAADF STEM) image of the film and (d) result from EDX line scan along the A-A′ line in the STEM image of (c). The black, blue, orange, and green dots denote the spectra from Si, Co, Cu, and Pt, respectively. The orange open circles denote the spectra from Bi.

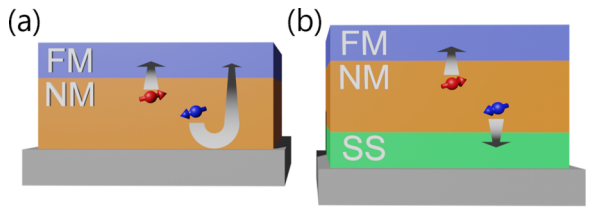

FIG. 3. Schematics of (a) spin backflow and (b) the effect of introducing a spin sink (SS) layer. The spin current is generated in the nonmagnet (NM) layer by the spin Hall effect and spin angular momenta injected into the ferromagnet (FM) layer. When the spin diffusion length in the NM layer is much longer than its thickness, spin angular momenta with opposite directions are reflected at the interface between the NM layer and substrate, resulting in spin backflow to the FM layer. By introducing the SS layer beneath the NM layer, the spins flowing into the SS layer can relax because of its spin-orbit interaction and the spin backflow is suppressed.

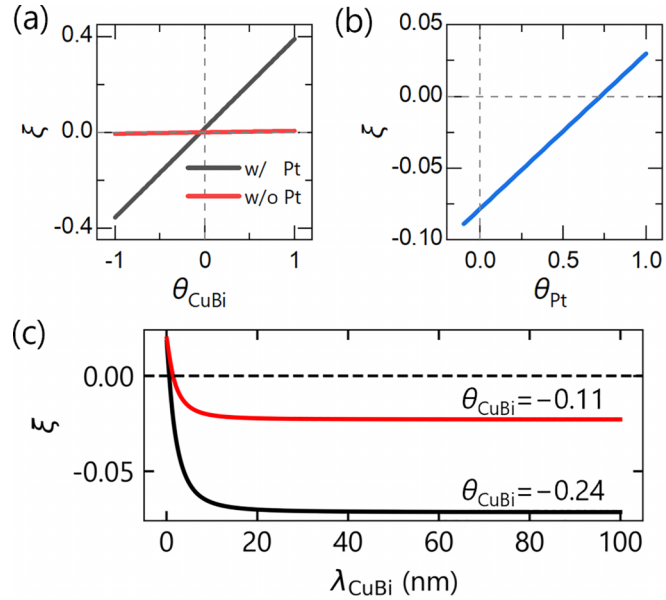

FIG. 4. (a) Calculation results of the relationship between the spin-orbit torque (SOT) efficiency ξ and spin Hall angle (θ) of the CuBi layer θ_{CuBi} with θ of the Pt layer $\theta_{Pt} = 0.062$ in a Co/CuBi/Pt trilayer. The black and red solid lines show the results for the thickness of the Pt $t_{Pt} = 5$ and 0 nm, respectively. (b) Calculation results of the relationship between ξ and θ_{Pt} when θ_{CuBi} is set at -0.24. The SOT efficiency is defined as the ratio of spin current at the Co/CuBi interface to the charge current through the CuBi and Pt layers. (c) Calculation results of the relationships between ξ and λ_{CuBi}. The black and red solid lines show the results for the spin Hall angle of CuBi. θ_{CuBi} is set at -0.24 and -0.11, respectively. See the main text for details of the other parameters used for the calculations.

$\lambda_{Co} = 2.0$ nm [42] and $\lambda_{Pt} = 1.6$ nm [12], respectively. The spin diffusion length of CuBi was set as $\lambda_{CuBi} = 45$ nm [23] and the spin Hall angles of Co and Pt were set as $\theta_{Co} = 0.092$ [43] and $\theta_{Pt} = 0.062$ [12], respectively. Figure 4(a) shows the SOT efficiency (ξ) calculated as a function of the spin Hall angle of CuBi (θ_{CuBi}) for the structures with and without an SS layer. Here, ξ is defined as the spin current density injected into the FM layer divided by the average current density in the CuBi and Pt layers (see Supplemental Material, Sec. B [37] for details of the estimation of the SOT for a trilayer system). ξ of Co(5)/$Cu_{99.5}Bi_{0.5}$(5) is calculated to be around -0.01 even if θ_{CuBi} is set to -1.0, which is in principle smaller than the detectable limit in SOT measurements. Meanwhile, ξ of Co(5)/$Cu_{99.5}Bi_{0.5}$(5)/Pt(5) is calculated to be of the order of 0.1 because of the suppression of the spin backflow by the Pt layer. These results rationalize that the Pt layer works as an SS and enables observation of the SOT originating from the spin Hall effect (SHE) in CuBi. Although the spin current generated in Pt may affect the SOT in Co(5)/$Cu_{99.5}Bi_{0.5}$(5)/Pt(5), ξ of this structure is calculated to be negative even if the spin Hall angle of Pt is increased up to 0.6, as shown in Fig. 4(b), under the assumption of $\theta_{CuBi} = -0.24$ [23]. This is because most of the electric current is shunted through the CuBi layer owing to its high conductivity. Given that the spin Hall angle of Pt is expected to be at most 0.1 [7–12], ξ should be negative

in Co(5)/$Cu_{99.5}Bi_{0.5}$(5)/Pt(5) if the spin Hall angle of CuBi is negative and large, as reported previously [23].

Here, it is notable that we postulated the spin diffusion length of CuBi is dependent on the Bi composition itself; i.e., the spin scattering in CuBi is governed by incorporated Bi as a scattering center. In the case that the spin relaxation mechanism in CuBi is the Elliott-Yefet type, the spin diffusion length of our $Cu_{99.5}Bi_{0.5}$ ($\rho_{\mathrm{CuBi}} = 20.8\,\mu\Omega\,\mathrm{cm}$) is about 27 nm from the relation of the spin diffusion length of $Cu_{1-x}Bi_x$ and its resistivity [23]. To clarify how the λ_{CuBi} affects the SOT efficiency, a model calculation was implemented [see Fig. 4(c)]. In the small λ_{CuBi} region ($\lambda_{\mathrm{CuBi}} < \sim 15\,\mathrm{nm}$), ξ monotonically and rapidly changes as λ_{CuBi} increases. Meanwhile, in the long λ_{CuBi} region ($\lambda_{\mathrm{CuBi}} > \sim 15\,\mathrm{nm}$), ξ is almost constant. The calculation result unequivocally signifies that the SOT efficiency does not largely change even when shorter spin diffusion length such as 27 nm is assumed. To obtain further insight, the same calculation was carried out by assuming the spin Hall angle to be -0.11 [23]. The general trend of the SOT efficiency is the same as that using the spin Hall angle of -0.24. These model calculations underscore the validity of the insertion of Pt as the SS layer for SOT measurements; i.e., SOT from CuBi is not observed without the Pt SS layer due to the large spin diffusion length in CuBi and the insertion of Pt as the SS layer impedes the unwanted spin backflow. In short, the spin backflow in the CuBi layer due to its long spin diffusion length is suppressed by adding the Pt SS layer and negative SOT is expected in our Co/CuBi/Pt trilayer structure from our spin diffusion model; i.e., negative SOT from SHE in CuBi surmounts the positive SOT from SHE in Pt, when only the SHE in each layer is considered.

STFMR measurements were carried out to observe the SOT in Co(5)/$Cu_{99.5}Bi_{0.5}$(5)/Pt(5). The STFMR spectra measured for Co(5)/$Cu_{99.5}Bi_{0.5}$(5)/Pt(5) and Co(5)/Cu(5)/Pt(5) are shown in Figs. 5(a) and 5(b), respectively. The frequency was 12 GHz and $\phi = 45°$. The resonance spectra were fitted using the following function [9],

$$V_{\mathrm{dc}} = A\frac{(B_{\mathrm{ext}} - B_{\mathrm{res}})\Delta}{(B_{\mathrm{ext}} - B_{\mathrm{res}})^2 + \Delta^2} + S\frac{\Delta^2}{(B_{\mathrm{ext}} - B_{\mathrm{res}})^2 + \Delta^2} + aB_{\mathrm{ext}} + b, \quad (1)$$

where B_{res} is the resonance field, Δ is half width at half maximum of the Lorentzian, and $aB_{\mathrm{ext}} + b$ is the linear offset. As shown in Figs. 5(a) and 5(b), the STFMR spectra were fitted by Eq. (1) and deconvoluted into antisymmetric (the A part) and symmetric (the S part) Lorentzian components. Here, A and S are the coefficients of the A and S parts, respectively, and they exhibit the following ϕ dependence [18,44],

$$A = A_0\sin2\phi\cos\phi + A_1\sin2\phi + A_2\sin2\phi\sin\phi, \quad (2a)$$

$$S = S_0\sin2\phi\cos\phi + S_1\sin2\phi + S_2\sin2\phi\sin\phi + S_3\sin\phi, \quad (2b)$$

where A_0 is the signal amplitude attributed to the Oersted field along the y axis and fieldlike torque caused by the y-directed spins. S_0 is that attributed to the dampinglike torque due to the y-directed spins. Other coefficients represent SOT caused by the x- or z-directed spins and/or thermal contributions [18,44]. Figures 5(c) and 5(d) show the angular dependences of A and S for the Co(5)/$Cu_{99.5}Bi_{0.5}$(5)/Pt(5) and Co(5)/Cu(5)/Pt(5) devices at 12 GHz, respectively. Fitting curves were obtained using Eq. (2) considering the angle misalignment δ in ϕ. δ was determined in the fitting of coefficient A and was fixed in the fitting of coefficient S. The angular dependences of both A and S were fitted by Eq. (2), and it was found that A_0 and S_0 are dominant.

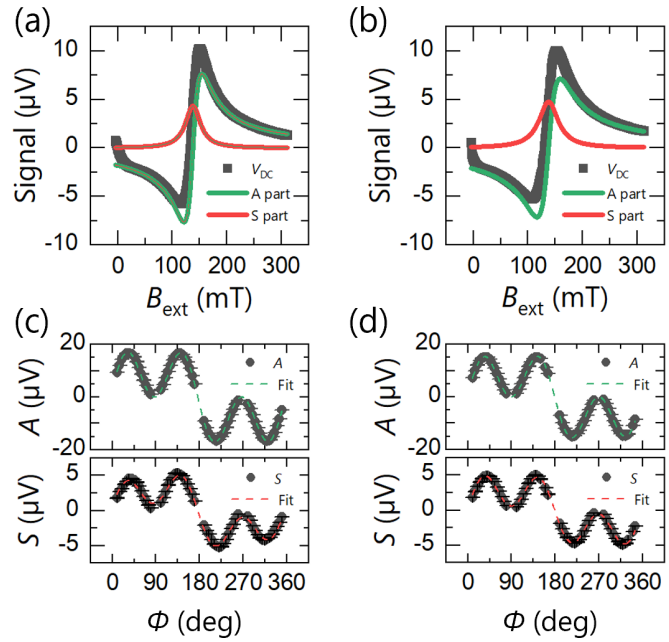

FIG. 5. STFMR spectra of (a) Co(5)/$Cu_{99.5}Bi_{0.5}$(5)/Pt(5) and (b) Co(5)/Cu(5)/Pt(5). Spectra were deconvoluted into a symmetric Lorentzian component (red solid lines) and antisymmetric Lorentzian component (green solid lines) using Eq. (1). The linear offset in the spectra has been subtracted. The parameters are obtained to be $B_{\mathrm{res}} = 137.85 \pm 0.02$ mT and $\Delta = 16.52 \pm 0.02$ mT for Co(5)/$Cu_{99.5}Bi_{0.5}$(5)/Pt(5), and $B_{\mathrm{res}} = 137.66 \pm 0.03$ mT and $\Delta = 21.25 \pm 0.03$ mT for Co(5)/Cu(5)/Pt(5), respectively. From the frequency dependence of the FMR spectra, $\mu_0 M_s$ is estimated to be 1.213 ± 0.002 T for Co(5)/$Cu_{99.5}Bi_{0.5}$(5)/Pt(5), and 1.195 ± 0.003 T for Co(5)/Cu(5)/Pt(5), respectively. The angular dependence of coefficients A and S at 12 GHz for (c) Co(5)/$Cu_{99.5}Bi_{0.5}$(5)/Pt(5) and (d) Co(5)/Cu(5)/Pt(5). Error bars represent the standard error obtained from fittings of the STFMR spectra for each angle. The amplitudes are obtained to be $A_0 = 22.1 \pm 0.2\,\mu\mathrm{V}$, $A_1 = -0.02 \pm 0.1\,\mu\mathrm{V}$, $A_2 = 0.2 \pm 0.2\,\mu\mathrm{V}$, $S_0 = 5.2 \pm 0.2\,\mu\mathrm{V}$, $S_1 = -0.44 \pm 0.07\,\mu\mathrm{V}$, $S_2 = 0.05 \pm 0.1\,\mu\mathrm{V}$, and $S_3 = 1.0 \pm 0.1\,\mu\mathrm{V}$ for Co(5)/$Cu_{99.5}Bi_{0.5}$(5)/Pt(5), and $A_0 = 19.9 \pm 0.1\,\mu\mathrm{V}$, $A_1 = -0.12 \pm 0.07\,\mu\mathrm{V}$, $A_2 = 0.19 \pm 0.09\,\mu\mathrm{V}$, $S_0 = 5.8 \pm 0.1\,\mu\mathrm{V}$, $S_1 = 0.10 \pm 0.05\,\mu\mathrm{V}$, $S_2 = 0.02 \pm 0.08\,\mu\mathrm{V}$, and $S_3 = 0.57 \pm 0.09\,\mu\mathrm{V}$ for Co(5)/Cu(5)/Pt(5), respectively. When calculating SOT efficiency ξ_{FMR} from S_0 and A_0, a standard error was introduced into resonance field B_{res} to reflect its angular dependence.

The SOT efficiency ξ_{FMR} was calculated using the following equation [9,45],

$$\xi_{\mathrm{FMR}} = \frac{e\mu_0 M_s t_{\mathrm{NM+SS}} t_{\mathrm{FM}}}{\hbar}\frac{S_0}{A_0}\sqrt{1 + \frac{\mu_0 M_{\mathrm{eff}}}{B_{\mathrm{res}}}}, \quad (3)$$

where e is elementary charge, $\hbar$ is the Dirac constant, $\mu_0 M_s$ is the saturation magnetization of the FM layer, t_{FM} is the thickness of the FM layer, and $t_{\mathrm{NM+SS}}$ is the sum of the NM

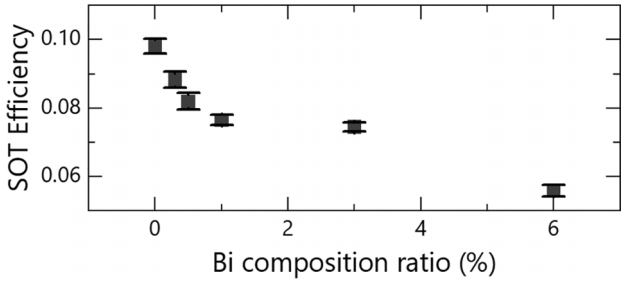

FIG. 6. Dependence of the SOT efficiency of Co/CuBi/Pt trilayer structures on the Bi composition ratio obtained from the STFMR measurements.

and SS layer thicknesses. $\mu_0 M_{\text{eff}}$ is the demagnetization field estimated by the Kittel formula, $f = \frac{\gamma}{2\pi}\sqrt{B_{\text{res}}(B_{\text{res}} + \mu_0 M_{\text{eff}})}$ [46], in the FMR measurements, where γ is the gyromagnetic ratio of an electron and f is the frequency. Figure 6 presents ξ_{FMR} for the Co/CuBi/Pt structures with different Bi compositions. Unlike the results for the Bi composition dependence of the spin Hall resistivity of CuBi obtained using the spin absorption method [23], ξ_{FMR} monotonically decreases as Bi composition increases. Importantly, the sign of ξ_{FMR} is positive within our experimental window.

To obtain further evidence for the results of the STFMR measurements, SHH measurements were conducted. The SHH voltage $V_{2\omega}$ is described as [47]

$$V_{2\omega} = A_{\text{DL}} \cos\phi + A_{\text{FL}} \cos\phi \cos 2\phi + V_{\text{PNE}} \sin 2(\phi - \delta_1) + C, \tag{4a}$$

$$A_{\text{DL}} = \frac{R_{\text{AHE}} I_0}{2} \frac{B_{\text{DL}}}{B_{\text{ext}} + B_{\text{K}}} + a_{\text{ONE}} B_{\text{ext}} + b_{\text{ANE}}, \tag{4b}$$

where A_{FL} is the signal amplitude generated by the fieldlike torque and C is the offset. $V_{\text{PNE}}\sin 2(\phi - \delta_1)$ is the planar Nernst effect [48] caused by the in-plane temperature gradient and δ_1 is the deviation of the temperature gradient from the y direction. $a_{\text{ONE}} B_{\text{ext}} + b_{\text{ANE}}$ represents the thermal effects of the anomalous and ordinary Nernst effects [47]. Figure 7(a) shows the ϕ dependence of the SHH voltages at 1 T for the Co(5)/$Cu_{99.5}Bi_{0.5}$(5)/Pt(5) structure, which is fitted by Eq. (4a). Figure 7(b) shows the B_{ext} dependence of A_{DL} for Co(5)/$Cu_{99.5}Bi_{0.5}$(5)/Pt(5), which is well fitted by Eq. (4b). Here, the anomalous Hall resistance (R_{AHE}) and effective field (B_{K}) were determined by measuring the anomalous Hall effect of the Co layer. As described in Eq. (4b), because the dampinglike SOT makes a nonlinear contribution to B_{ext}, the enhancement of A_{DL} in the low B_{ext} region signifies successful observation of SOT and thus the dampinglike effective field (B_{DL}) was estimated. The dampinglike torque efficiency was calculated using the following equation [45],

$$\xi_{\text{DL}} = \frac{2eM_s t_{\text{FM}} B_{\text{DL}}}{\hbar J_{\text{NM+SS}}}, \tag{5}$$

where $J_{\text{NM+SS}}$ is the average current density in the NM and the SS layers. The dependence of the dampinglike torque efficiency on the Bi composition of CuBi estimated using Eq. (5) is displayed in Fig. 7(c). The SOT efficiency decreased monotonically as Bi composition increased, which is consistent with the STFMR results shown in Fig. 6. Therefore,

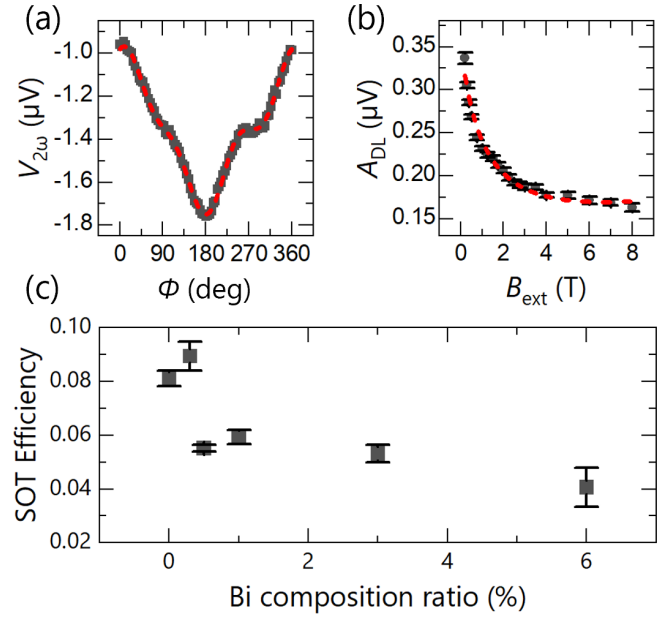

FIG. 7. (a) Second harmonic Hall (SHH) voltages obtained in Co(5)/$Cu_{99.5}Bi_{0.5}$(5)/Pt(5) when the external field B_{ext} was 1 T. The red dashed line shows the fitting result obtained using Eq. (4a). The amplitudes are obtained to be $A_{\text{DL}} = 231 \pm 3$ nV, $A_{\text{FL}} = 156 \pm 4$ nV, and $V_{\text{PNE}} = 40 \pm 2$ nV. (b) Dependence of the coefficient A_{DL} on B_{ext}. The fitting result was obtained using Eq. (4b). The parameters are obtained to be $B_{\text{DL}} = 0.55 \pm 0.04$ mT, $a_{\text{ONE}} = 5 \pm 2$ nV/T, and $b_{\text{ANE}} = (10 \pm 1) \times 10$ nV. $R_{\text{AHE}} = 55$ mΩ and $B_{\text{K}} = 1.19$ T are used for this fitting. (c) Dependence of the SOT efficiency on the Bi composition ratio obtained from the SHH measurements. The angle misalignment of the second harmonic voltages was obtained by fitting the first harmonic voltage at 1 T measured simultaneously.

the positive SOT efficiency in addition to the monotonic decrease of the SOT efficiency of CuBi are corroborated by the results shown in Fig. 7. Furthermore, considering the relationship between ξ and θ_{Pt} shown in Fig. 4(b), we emphasize that the positive ξ of CuBi determined in this study is not ascribed to the positive θ_{Pt} because θ_{Pt} that is greater than 0.6 is needed to achieve positive ξ; i.e., the Pt SS layer does not contribute to the positive ξ of CuBi.

To unveil the origin of the positive SOT efficiency of the Co/CuBi/Pt structure, we consider the possible contribution from the OHE of Cu. The OHE is the phenomenon where orbital angular momentum propagates perpendicular to the external electric field direction, which is reminiscent of the SHE. A notable physical trait of the OHE is that it is observed even in light elements. Among elements displaying a substantial OHE, Cu exhibits positive and large orbital Hall conductivity [49–51]. Therefore, the OHE of CuBi might produce sizable positive orbital torque (see also Supplemental Material, Sec. C [37] for the results of both the STFMR and SHH measurements of Co/CuBi bilayer devices). Investigation of the SOT of a structure with a different FM is one approach to verify the contribution from the OHE, because the magnitude of orbital torque is known to depend on the orbital to spin conversion efficiency in an FM layer, i.e., the orbital susceptibility [52]. Py is known to have weaker orbital susceptibility than Co [52–54], so the SOT efficiency

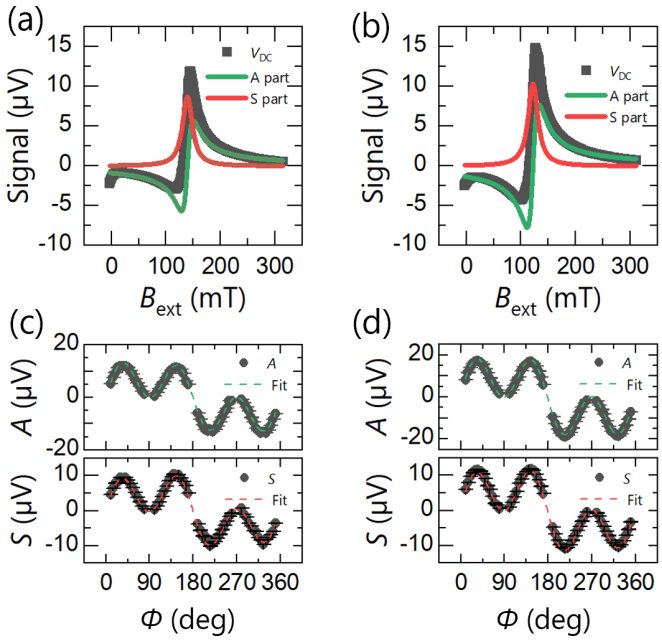

FIG. 8. STFMR results for (a) Py(5)/$Cu_{99.5}Bi_{0.5}$(5)/Pt(5) and (b) Py(5)/Cu(5)/Pt(5) structures. The spectra were deconvoluted into a symmetric Lorentzian part (red solid line) and antisymmetric Lorentzian part (green solid line) using Eq. (1). The linear offset in the spectra has been subtracted. The parameters are obtained to be $B_{res} = 139.45 \pm 0.02$ mT and $\Delta = 10.87 \pm 0.02$ mT for Py(5)/$Cu_{99.5}Bi_{0.5}$(5)/Pt(5), and $B_{res} = 122.04 \pm 0.02$ mT and $\Delta = 10.77 \pm 0.02$ mT for Py(5)/Cu(5)/Pt(5), respectively. From the frequency dependence of FMR spectra, $\mu_0 M_s$ is estimated to be 0.446 ± 0.002 T for Co(5)/$Cu_{99.5}Bi_{0.5}$(5)/Pt(5), and 0.556 ± 0.003 T for Co(5)/Cu(5)/Pt(5), respectively. Angular dependence of coefficients A and S at 8 GHz of (c) Py(5)/$Cu_{99.5}Bi_{0.5}$(5)/Pt(5) and (d) Py(5)/Cu(5)/Pt(5) structures. The amplitudes are obtained to be $A_0 = 16.5 \pm 0.2\,\mu$V, $A_1 = 0.3 \pm 0.1\,\mu$V, $A_2 = 0.2 \pm 0.2\,\mu$V, $S_0 = 12.7 \pm 0.2\,\mu$V, $S_1 = -0.45 \pm 0.08\,\mu$V, $S_2 = 0.2 \pm 0.1\,\mu$V, and $S_3 = -0.4 \pm 0.1\,\mu$V for Py(5)/$Cu_{99.5}Bi_{0.5}$(5)/Pt(5), and $A_0 = 23.1 \pm 0.2\,\mu$V, $A_1 = 0.1 \pm 0.1\,\mu$V, $A_2 = 0.3 \pm 0.2\,\mu$V, $S_0 = 14.4 \pm 0.2\,\mu$V, $S_1 = -0.32 \pm 0.09\,\mu$V, $S_2 = 0.1 \pm 0.1\,\mu$V, and $S_3 = -0.07 \pm 0.2\,\mu$V for Py(5)/Cu(5)/Pt(5), respectively.

is expected to be suppressed by changing the FM layer from Co to Py in the OHE regime. We conducted STFMR measurements of Py(5)/$Cu_{99.5}Bi_{0.5}$(5)/Pt(5) and Py(5)/Cu(5)/Pt(5) devices (Fig. 8), which gave ξ_{FMR} of 0.074 ± 0.001 and 0.070 ± 0.001, respectively. Given that the contribution from the OHE is negligible in Py devices whereas it can be nonzero in Co devices, the slight decrease of ξ_{FMR} by 10%–29% in the Py devices compared with that of the Co devices indicates that the Co/CuBi/Pt devices exhibit a non-negligible OHE. It is notable that the decrement of the SOT efficiency under replacement of the FM layer from Co to Py is not completely explained by the spin memory loss [55,56]. A previous work clarified that the spin memory loss parameter δ at the Py/Cu interface and at the Co/Cu interface are quite small, ∼0 and 0.11, respectively [57]. Since the Bi composition ratio in CuBi is small enough, we deduce that the SMLs at Py/CuBi and at Co/CuBi are approximately negligible. However, the fact that the SOT of the Py devices is still sizable (71%–90% of the SOT in the Co devices) indicates that the OHE of Cu in CuBi is not a dominant contributor to the SOT of the FM/CuBi/Pt devices. It should be noted that the OHE of Pt does not allow sufficient SOT by the same reason, although the OHE of Pt is not negligible [49,50,58]. We also note that the spin Hall angle of Pt needs to be greater than 0.6 to attribute the SOT observed in the FM/CuBi/Pt device to the SHE of Pt [see also Fig. 4(b)].

TABLE I. List of the representative spin-orbit torque (SOT) efficiencies obtained by spin-torque ferromagnetic resonance (STFMR) measurement at room temperature.

Structure	SOT efficiency	Reference
$Ni_{81}Fe_{19}$(8)/Cu(10)	0.00087	[29]
Co(5)/Cu(5)/Pt(5)	0.098	Our work
Co(5)/$Cu_{99.5}Bi_{0.5}$(5)/Pt(5)	0.082	Our work
$Ni_{80}Fe_{20}$(5)/Cu(5)/Pt(5)	0.070	Our work
$Ni_{80}Fe_{20}$(5)/$Cu_{99.5}Bi_{0.5}$(5)/Pt(5)	0.074	Our work
$Co_{90}Fe_{10}$(6)/Pt(6)	0.077	[18]
$Ni_{81}Fe_{19}$(8)/Pt(6)	0.058	[18]
$Ni_{81}Fe_{19}$(5)/$Cu_{72}Pt_{28}$(6)	0.054	[35]

Because neither the SHE of CuBi and Pt nor the OHE of Cu and Pt explains the positive SOT of the FM/CuBi/Pt devices, the charge to spin conversion caused by the Rashba effect at the FM/CuBi interface and/or that at the CuBi/Pt interface enables the positive SOT. The Rashba effect at the FM/CuBi interface is negligible because the SOT of FM/CuBi without a Pt SS layer is negligible (see Supplemental Material, Sec. C [37]). The SOT from the FM/CuBi interface should be sizable if the Rashba effect at the FM/CuBi interface is dominant, but this is not the case. Therefore, the Rashba effects at the CuBi/Pt interface can be a pivotal source of the positive SOT of FM/CuBi/Pt, which surmounts the output of the negative SHE of CuBi. Indeed, several previous studies revealed the strong Rashba effect at the Cu/Pt interface [55,59–62], supporting our assertion. The Bi composition dependence of the SOT efficiency can be explained within this scheme, because the increase of the Bi composition of CuBi invokes monotonic suppression of the spin diffusion length of CuBi and the amount of spin current due to the Rashba effect at the CuBi/Pt interface that can reach the top FM layer also decreases monotonically. From the discussion above, the whole result can be rationalized as the negative SHE of CuBi contributes the SOT due to the Pt spin sink layer but it is surmounted by the positive Rashba effect at the CuBi/Pt interface. The positive contributions from the OHE in CuBi and Pt are found to be nonzero but much smaller than that from the Rashba effect at the CuBi/Pt interface. For reference, representative SOT efficiencies in previous works and our characteristic SOT efficiencies are briefly summarized in Table I. The SOTs from FM/Pt bilayers are comparable to that of the FM/Cu(CuBi)/Pt trilayer. Given that the CuBi exhibits subsequent (negative) spin Hall angle, all the results signify that additional contribution of the Rashba effect at the CuBi/Pt interface is dominant in SOT. Here, we note that it is possible Cu:Pt alloy formation is not completely negated in the TEM and EDX studies as described above, although no direct evidence of the Cu:Pt formation was obtained. Cu:Pt

can exhibit the spin Hall angle of, at maximum, ∼0.08 [35], which may contribute to the SOT in the FM/CuBi/Pt. Hence, although we did not take the SOT from the Cu:Pt into account in the estimation of the SOT, we emphasize that further study is necessary to clarify the possible formation of the Cu:Pt and its role in the SOT, which is quite helpful to obtain a more precise physical picture of the SOT in Cu-based spin devices.

IV. CONCLUSION

The STFMR and SHH measurements were conducted at room temperature to estimate SOT efficiency of CuBi, where the Bi atoms doped in Cu acted as spin scatterers. The measurements were performed using FM/CuBi/Pt trilayer structures, in which the Pt SS layer allowed observation of the SOT by suppressing unwanted spin backflow. Unlike a previous study using spin absorption, positive SOT was observed in our trilayer structure with a wide range of Bi compositions. Control experiments revealed that the spin current generated at the interface between the CuBi and Pt SS layers allowed the positive SOT in the FM/CuBi/Pt trilayer structure by surmounting the negative SOT from CuBi. Our study, however, does not signify that the sign of the SHE of CuBi is positive. Indeed, positive SOTs from the SHE in Pt and the Rashba effect at the Cu/Pt interface (and possibly the SHE from the Cu:Pt intermixing layer) are superposed to the negative SOT from CuBi by using Pt as an SS layer, without which one cannot detect sizable SOT from the FM/CuBi bilayer in the STFMR as discussed in Sec. III. Our findings substantiate that careful device design such as material selection for the SS layer is necessary to extract large SOT from CuBi in SOT devices and provide a path to use Bi-doped transition metals for practical spin-orbitronic applications.

ACKNOWLEDGMENTS

This work was partially supported by the Japan Society for the Promotion of Science (JSPS) Grant-in-Aid for Scientific Research (A) (Grant No. 23H00268) and the Spintronics Research Network of Japan (Spin-RNJ). We thank Masami Komoike and Satoshi Yamashita for their experimental assistance.

[1] J. E. Hirsch, Spin Hall effect, Phys. Rev. Lett. **83**, 1834 (1999).
[2] E. Saitoh, M. Ueda, H. Miyajima, and G. Tatara, Conversion of spin current into charge current at room temperature: Inverse spin-Hall effect, Appl. Phys. Lett. **88**, 182509 (2006).
[3] D. Hou, Z. Qiu, K. Harii, Y. Kajiwara, K. Uchida, Y. Fujiwara, H. Nakayama, T. Yoshino, T. An, K. Ando *et al.*, Interface induced inverse spin Hall effect in bismuth/permalloy bilayer, Appl. Phys. Lett. **101**, 042403 (2012).
[4] H. Emoto, Y. Ando, E. Shikoh, Y. Fuseya, T. Shinjo, and M. Shiraishi, Conversion of pure spin current to charge current in amorphous bismuth, J. Appl. Phys. **115**, 17C507 (2014).
[5] H. Emoto, Y. Ando, G. Eguchi, R. Ohshima, E. Shikoh, Y. Fuseya, T. Shinjo, and M. Shiraishi, Transport and spin conversion of multicarriers in semimetal bismuth, Phys. Rev. B **93**, 174428 (2016).
[6] M. Tokuda, N. Kabeya, K. Iwashita, H. Taniguchi, T. Arakawa, D. Yue, X. Gong, X. Jin, K. Kobayashi, and Y. Niimi, Spin transport measurements in metallic Bi/Ni nanowires, Appl. Phys. Express **12**, 053005 (2019).
[7] J. Sinova, S. O. Valenzuela, J. Wunderlich, C. H. Back, and T. Jungwirth, Spin Hall effects, Rev. Mod. Phys. **87**, 1213 (2015).
[8] O. Mosendz, V. Vlaminck, J. E. Pearson, F. Y. Fradin, G. E. W. Bauer, S. D. Bader, and A. Hoffmann, Detection and quantification of inverse spin Hall effect from spin pumping in permalloy/normal metal bilayers, Phys. Rev. B **82**, 214403 (2010).
[9] L. Liu, T. Moriyama, D. C. Ralph, and R. A. Buhrman, Spin-torque ferromagnetic resonance induced by the spin Hall effect, Phys. Rev. Lett. **106**, 036601 (2011).
[10] W. Zhang, W. Han, X. Jiang, S.-H. Yang, and S. S. P. Parkin, Role of transparency of platinum–ferromagnet interfaces in determining the intrinsic magnitude of the spin Hall effect, Nat. Phys. **11**, 496 (2015).
[11] C.-F. Pai, Y. Ou, L. H. Vilela-Leão, D. C. Ralph, and R. A. Buhrman, Dependence of the efficiency of spin Hall torque on the transparency of Pt/ferromagnetic layer interfaces, Phys. Rev. B **92**, 064426 (2015).
[12] E. Sagasta, Y. Omori, M. Isasa, M. Gradhand, L. E. Hueso, Y. Niimi, Y. C. Otani, and F. Casanova, Tuning the spin Hall effect of Pt from the moderately dirty to the superclean regime, Phys. Rev. B **94**, 060412(R) (2016).
[13] L. Liu, C.-F. Pai, Y. Li, H. W. Tseng, D. C. Ralph, and R. A. Buhrman, Spin-torque switching with the giant spin Hall effect of tantalum, Science **336**, 555 (2012).
[14] E. Sagasta, Y. Omori, S. Vélez, R. Llopis, C. Tollan, A. Chuvilin, L. E. Hueso, M. Gradhand, Y. C. Otani, and F. Casanova, Unveiling the mechanisms of the spin Hall effect in Ta, Phys. Rev. B **98**, 060410(R) (2018).
[15] C.-F. Pai, L. Liu, Y. Li, H. W. Tseng, D. C. Ralph, and R. A. Buhrman, Spin transfer torque devices utilizing the giant spin Hall effect of tungsten, Appl. Phys. Lett. **101**, 122404 (2012).
[16] D. Yue, W. Lin, J. Li, X. Jin, and C. L. Chien, Spin-to-charge conversion in Bi films and Bi/Ag bilayers, Phys. Rev. Lett. **121**, 037201 (2018).
[17] N. Fukumoto, R. Ohshima, M. Aoki, Y. Fuseya, M. Matsushima, E. Shigematsu, T. Shinjo, Y. Ando, S. Sakamoto, M. Shiga *et al.*, Observation of large spin conversion anisotropy in bismuth, Proc. Natl. Acad. Sci. USA **120**, e2215030120 (2023).
[18] S. Karimeddiny, J. A. Mittelstaedt, R. A. Buhrman, and D. C. Ralph, Transverse and longitudinal spin-torque ferromagnetic resonance for improved measurement of spin-orbit torque, Phys. Rev. Appl. **14**, 024024 (2020).
[19] U. H. Pi, K. W. Kim, J. Y. Bae, S. C. Lee, Y. J. Cho, K. S. Kim, and S. Seo, Tilting of the spin orientation induced by Rashba effect in ferromagnetic metal layer, Appl. Phys. Lett. **97**, 162507 (2010).
[20] M. Hayashi, J. Kim, M. Yamanouchi, and H. Ohno, Quantitative characterization of the spin-orbit torque using harmonic Hall voltage measurements, Phys. Rev. B **89**, 144425 (2014).

[21] Y. Wen, J. Wu, P. Li, Q. Zhang, Y. Zhao, A. Manchon, J. Q. Xiao, and X. Zhang, Temperature dependence of spin-orbit torques in Cu-Au alloys, Phys. Rev. B **95**, 104403 (2017).

[22] M. Gradhand, D. V. Fedorov, P. Zahn, and I. Mertig, Spin Hall angle versus spin diffusion length: Tailored by impurities, Phys. Rev. B **81**, 245109 (2010).

[23] Y. Niimi, Y. Kawanishi, D. H. Wei, C. Deranlot, H. X. Yang, M. Chshiev, T. Valet, A. Fert, and Y. Otani, Giant spin Hall effect induced by skew scattering from bismuth impurities inside thin film CuBi alloys, Phys. Rev. Lett. **109**, 156602 (2012).

[24] D. V. Fedorov, C. Herschbach, A. Johansson, S. Ostanin, I. Mertig, M. Gradhand, K. Chadova, D. Ködderitzsch, and H. Ebert, Analysis of the giant spin Hall effect in Cu(Bi) alloys, Phys. Rev. B **88**, 085116 (2013).

[25] P. M. Levy, H. Yang, M. Chshiev, and A. Fert, Spin Hall effect induced by Bi impurities in Cu: Skew scattering and side-Jump, Phys. Rev. B **88**, 214432 (2013).

[26] Y. Niimi, H. Suzuki, Y. Kawanishi, Y. Omori, T. Valet, A. Fert, and Y. Otani, Extrinsic spin Hall effects measured with lateral spin valve structures, Phys. Rev. B **89**, 054401 (2014).

[27] B. Gu, Z. Xu, M. Mori, T. Ziman, and S. Maekawa, Enhanced spin Hall effect by electron correlations in CuBi alloys, J. Appl. Phys. **117**, 17D503 (2015).

[28] S. Ruiz-Gómez, R. Guerrero, M. W. Khaliq, C. Fernández-González, J. Prat, A. Valera, S. Finizio, P. Perna, J. Camarero, L. Pérez *et al.*, Direct x-ray detection of the spin hall effect in CuBi, Phys. Rev. X **12**, 031032 (2022).

[29] H. An, Y. Kageyama, Y. Kanno, N. Enishi, and K. Ando, Spin–torque generator engineered by natural oxidation of Cu, Nat. Commun. **7**, 13069 (2016).

[30] S. Ding, A. Ross, D. Go, L. Baldrati, Z. Ren, F. Freimuth, S. Becker, F. Kammerbauer, J. Yang, G. Jakob *et al.*, Harnessing orbital-to-spin conversion of interfacial orbital currents for efficient spin-orbit torques, Phys. Rev. Lett. **125**, 177201 (2020).

[31] E. Santos, J. E. Abrão, A. S. Vieira, J. B. S. Mendes, R. L. Rodríguez-Suárez, and A. Azevedo, Exploring orbital-charge conversion mediated by interfaces with CuO_x through spin-orbital pumping, Phys. Rev. B **109**, 014420 (2024).

[32] H. Kontani, T. Tanaka, D. S. Hirashima, K. Yamada, and J. Inoue, Giant orbital Hall effect in transition metals: Origin of large spin and anomalous Hall effects, Phys. Rev. Lett. **102**, 016601 (2009).

[33] Y. Niimi, M. Morota, D. H. Wei, C. Deranlot, M. Basletic, A. Hamzic, A. Fert, and Y. Otani, Extrinsic spin Hall effect induced by iridium impurities in copper, Phys. Rev. Lett. **106**, 126601 (2011).

[34] S. Takizawa, M. Kimata, Y. Omori, Y. Niimi, and Y. Otani, Spin mixing conductance in Cu–Ir dilute alloys, Appl. Phys. Express **9**, 063009 (2016).

[35] R. Ramaswamy, Y. Wang, M. Elyasi, M. Motapothula, T. Venkatesan, X. Qiu, and H. Yang, Extrinsic spin Hall effect in $Cu_{1-x}Pt_x$, Phys. Rev. Appl. **8**, 024034 (2017).

[36] F. Rortais, S. Lee, R. Ohshima, S. Dushenko, Y. Ando, and M. Shiraishi, Spin-orbit coupling induced by bismuth doping in silicon thin films, Appl. Phys. Lett. **113**, 122408 (2018).

[37] See Supplemental Material at http://link.aps.org/supplemental/10.1103/PhysRevB.110.094419 for the details of the estimation of the SOT for a trilayer system, the results of the both the STFMR and the SHH measurements of the Co/CuBi bilayer devices, the results of the STFMR measurement of the Py/CuBi bilayer devices, and details of the interpretation of the EDX signal, which includes Refs. [38,39].

[38] D. B. Williams and C. B. Carter, *The Transmission Electron Microscope* (Plenum Press, New York, 1996), Chap. 36, pp. 623–626.

[39] *Introduction to Analytical Electron Microscopy*, edited by J. J. Hren, J. I. Goldstein, and D. C. Joy (Plenum Press, New York, 1979), pp. 101–102.

[40] H. Xue, M. Tang, Y. Zhang, Z. Ji, X. Qiu, and Z. Zhang, Giant enhancement of spin-orbit torque efficiency in Pt/Co bilayers by inserting a WSe_2 under layer, Adv. Electron. Mater. **8**, 2100684 (2022).

[41] A. Fert and H. Jaffrès, Conditions for efficient spin injection from a ferromagnetic metal into a semiconductor, Phys. Rev. B **64**, 184420 (2001).

[42] G. Zahnd, L. Vila, V. T. Pham, M. Cosset-Cheneau, W. Lim, A. Brenac, P. Laczkowski, A. Marty, and J. P. Attané, Spin diffusion length and polarization of ferromagnetic metals measured by the spin-absorption technique in lateral spin valves, Phys. Rev. B **98**, 174414 (2018).

[43] Y. Omori, E. Sagasta, Y. Niimi, M. Gradhand, L. E. Hueso, F. Casanova, and Y. C. Otani, Relation between spin Hall effect and anomalous Hall effect in 3*d* ferromagnetic metals, Phys. Rev. B **99**, 014403 (2019).

[44] M. Aoki, E. Shigematsu, R. Ohshima, T. Shinjo, M. Shiraishi, and Y. Ando, Current-induced out-of-plane torques in a single permalloy layer with lateral structural asymmetry, Phys. Rev. B **105**, 144407 (2022).

[45] M.-H. Nguyen and C.-F. Pai, Spin–orbit torque characterization in a nutshell, APL Mater. **9**, 030902 (2021).

[46] C. Kittel, On the theory of ferromagnetic resonance absorption, Phys. Rev. **73**, 155 (1948).

[47] N. Roschewsky, E. S. Walker, P. Gowtham, S. Muschinske, F. Hellman, S. R. Bank, and S. Salahuddin, Spin-orbit torque and Nernst effect in Bi-Sb/Co heterostructures, Phys. Rev. B **99**, 195103 (2019).

[48] A. D. Avery, M. R. Pufall, and B. L. Zink, Observation of the planar Nernst effect in permalloy and nickel thin films with in-plane thermal gradients, Phys. Rev. Lett. **109**, 196602 (2012).

[49] D. Jo, D. Go, and H.-W. Lee, Gigantic intrinsic orbital Hall effects in weakly spin-orbit coupled metals, Phys. Rev. B **98**, 214405 (2018).

[50] L. Salemi and P. M. Oppeneer, First-principles theory of intrinsic spin and orbital Hall and Nernst effects in metallic monoatomic crystals, Phys. Rev. Mater. **6**, 095001 (2022).

[51] A. Rothschild, N. Am-Shalom, N. Bernstein, M. Meron, T. David, B. Assouline, E. Frohlich, J. Xiao, B. Yan, and A. Capua, Generation of spin currents by the orbital Hall effect in Cu and Al and their measurement by a Ferris-wheel ferromagnetic resonance technique at the wafer level, Phys. Rev. B **106**, 144415 (2022).

[52] D. Lee, D. Go, H.-J. Park, W. Jeong, H.-W. Ko, D. Yun, D. Jo, S. Lee, G. Go, J. H. Oh *et al.*, Orbital torque in magnetic bilayers, Nat. Commun. **12**, 6710 (2021).

[53] S. Dutta and A. A. Tulapurkar, Observation of nonlocal orbital transport and sign reversal of dampinglike torque in Nb/Ni and Ta/Ni bilayers, Phys. Rev. B **106**, 184406 (2022).

[54] H. Hayashi, D. Jo, D. Go, T. Gao, S. Haku, Y. Mokrousov, H.-W. Lee, and K. Ando, Observation of long-range orbital transport and giant orbital torque, Commun. Phys. **6**, 32 (2023).

[55] J.-C. Rojas-Sánchez, N. Reyren, P. Laczkowski, W. Savero, J.-P. Attané, C. Deranlot, M. Jamet, J.-M. George, L. Vila, and H. Jaffrès, Spin pumping and inverse spin Hall effect in platinum: The essential role of spin-memory loss at metallic interfaces, Phys. Rev. Lett. **112**, 106602 (2014).

[56] X. Tao, Q. Liu, B. Miao, R. Yu, Z. Feng, L. Sun, B. You, J. Du, K. Chen, S. Zhang *et al.*, Self-consistent determination of spin Hall angle and spin diffusion length in Pt and Pd: The role of the interface spin loss, Sci. Adv. **4**, eaat1670 (2018).

[57] R. Liu, K. Gupta, Z. Yuan, and P. J. Kelly, Calculating the spin memory loss at Culmetal interfaces from first principles, Phys. Rev. B **106**, 014401 (2022).

[58] G. Sala and P. Gambardella, Giant orbital Hall effect and orbital-to-spin conversion in $3d$, $5d$, and $4f$ metallic heterostructures, Phys. Rev. Res. **4**, 033037 (2022).

[59] H. Kurt, R. Loloee, K. Eid, W. P. Pratt, and J. Bass, Spin-memory loss at 4.2 K in sputtered Pd and Pt and at Pd/Cu and Pt/Cu interfaces, Appl. Phys. Lett. **81**, 4787 (2002).

[60] K. Dolui and B. K. Nikolić, Spin-memory loss due to spin-orbit coupling at ferromagnet/heavy-metal interfaces: *Ab initio* spin-density matrix approach, Phys. Rev. B **96**, 220403(R) (2017).

[61] V. P. Amin, J. Zemen, and M. D. Stiles, Interface-generated spin currents, Phys. Rev. Lett. **121**, 136805 (2018).

[62] R. Yu, B. Miao, Q. Liu, K. He, W. Xue, L. Sun, M. Wu, Y. Wu, Z. Yuan, and H. Ding, Fingerprint of the inverse Rashba-Edelstein effect at heavy-metal/Cu interfaces, Phys. Rev. B **102**, 144415 (2020).